Supplementary Information

Nanocomposite Antimicrobials Prevent Bacterial Growth Through the Enzyme-like Activity of Bi-Doped Cerium Dioxide ($Ce_{1-x}Bi_xO_{2-\delta}$)

Hajo Frerichs,[†] Eva Pütz,[†] Felix Pfitzner,[†] Tobias Reich,[‡] Athanasios Gazanis,[$] Martin Panthöfer,[†] Jens Hartmann,[†] Olga Jegel,[†] Ralf Heermann[$] and Wolfgang Tremel[†]*

[†] Chemistry Department, Johannes Gutenberg-Universität Mainz, Duesbergweg 10-14, D-55128 Mainz, Germany

[‡] Chemistry Department, Johannes Gutenberg-Universität, Fritz-Strassmann-Weg 2, D-55128 Mainz, Germany.

[$] Institut für Molekulare Physiologie, Mikrobiologie und Weinforschung, Johannes-Gutenberg-Universität Mainz,Becherweg 15, D-55128 Mainz, Germany

Contents

Plots Rietveld Refinements

The powder diffraction data for Rietveld refinement were collected from samples prepared on polyvinyl acetate foil with Fomblin Y (average mole wt 3300). Table S1 shows the refined parameters. The Rietveld refinements (Figure S1) were done via Topas Academic v6[1,2] and based on the documented structure (International Crystal Structure Database (ICSD)) for pure CeO_2 (ICSD ID: 72155). Bi^{3+} was assumed to replace Ce^{4+} on the cation sites. Assumed spherical crystallites show crystallite diameters in the range of ~5 nm. Furthermore the refinements of both compositions showed a similar structural model with cubic symmetry (space group $Fm\bar{3}m$) with lattice parameters $a(CeO_{2-\delta})$ = 5.4325(2) Å and $a(Ce_{0.8}Bi_{0.2}O_{2-\delta})$ = 5.4552(1) Å (Table S1).

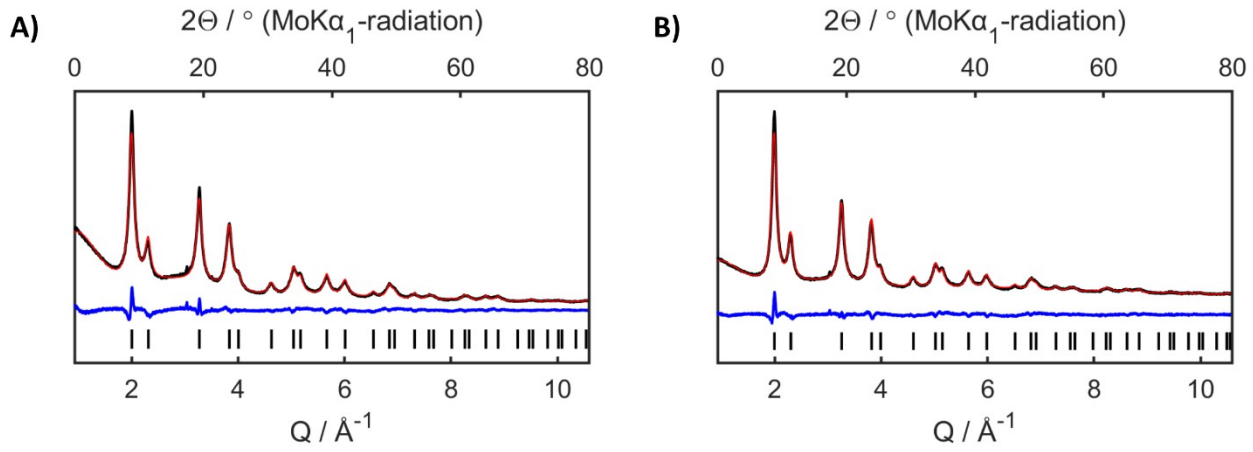

Figure S1. Rietveld refinements for (A) cerium oxide $CeO_{2-\delta}$. (B) substituted cerium bismuth oxide $Ce_{0.8}Bi_{0.2}O_{2-\delta}$.

EDX-Measurements

The EDX-spectra were obtained using the EDAX Pegasus X4M unit at a FEI Nova NanoSEM 630. The calibration was done by measuring copper foil on an alumina stab. The data processing and quantification was done with the EDAX Genesis software package. For this an acceleration voltage of 15 kV was applied to analyze the samples in depth. The silicon signal is due to the sample preparation on a silicon wafer.

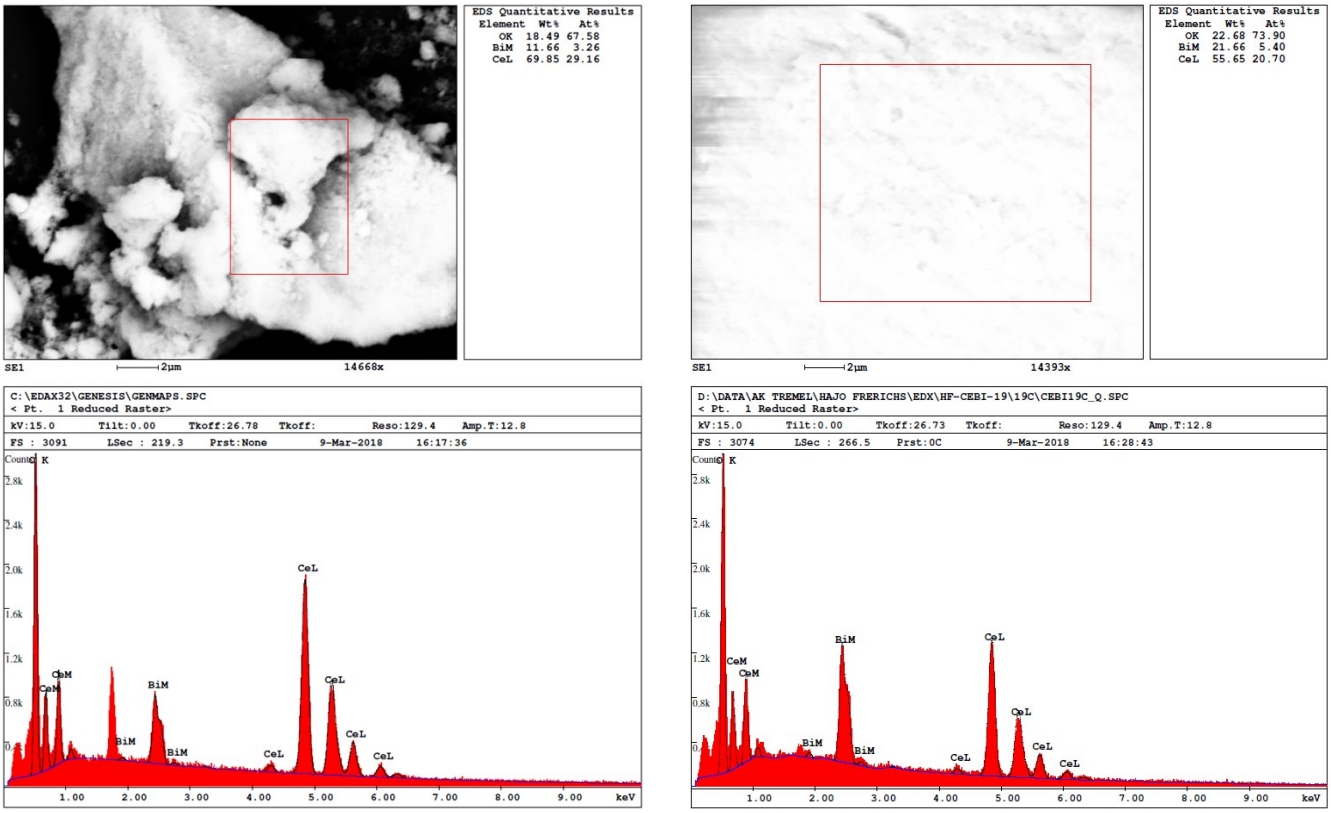

Figure S2. EDX quantification of $Ce_{o.9}Bi_{o.1}O_{1.95}$ (left) and $Ce_{0.8}Bi_{0.2}O_{1.90}$ (right).

From the EDX measurements the Ce:Bi ratios of both species were determined. For the nominal composition of $Ce_{0.9}Bi_{0.1}O_{1.95}$ a Ce:Bi ratio of 8.94 (nominal 9) (Ce 0.8994 / Bi 0.1006) and for the nominal composition of $Ce_{0.8}Bi_{0.2}O_{1.90}$ a Ce:Bi ratio of 3.83 (nominal 4) (Ce 0.7931 / Bi 0.2069) were found.

Quantification of the cerium and bismuth amount

The amount of cerium and bismuth was determined colometrically with external calibration.[3,4] For cerium, we utilized the specific reaction between cerium and 8-hydroxyquinoline was used. The specific reaction between xylenolorange and bismuth was used for the quantitive determination of the bismuth content. Figure S3 shows the spectra of both external calibration solutions together with the respective sample measurements. Both concentration series show an increasing absorbance with increasing metal concentration (A1 and B1). The metal determinations do not interfere with each other (A2 and B2), i.e., the determinations are metal specific.

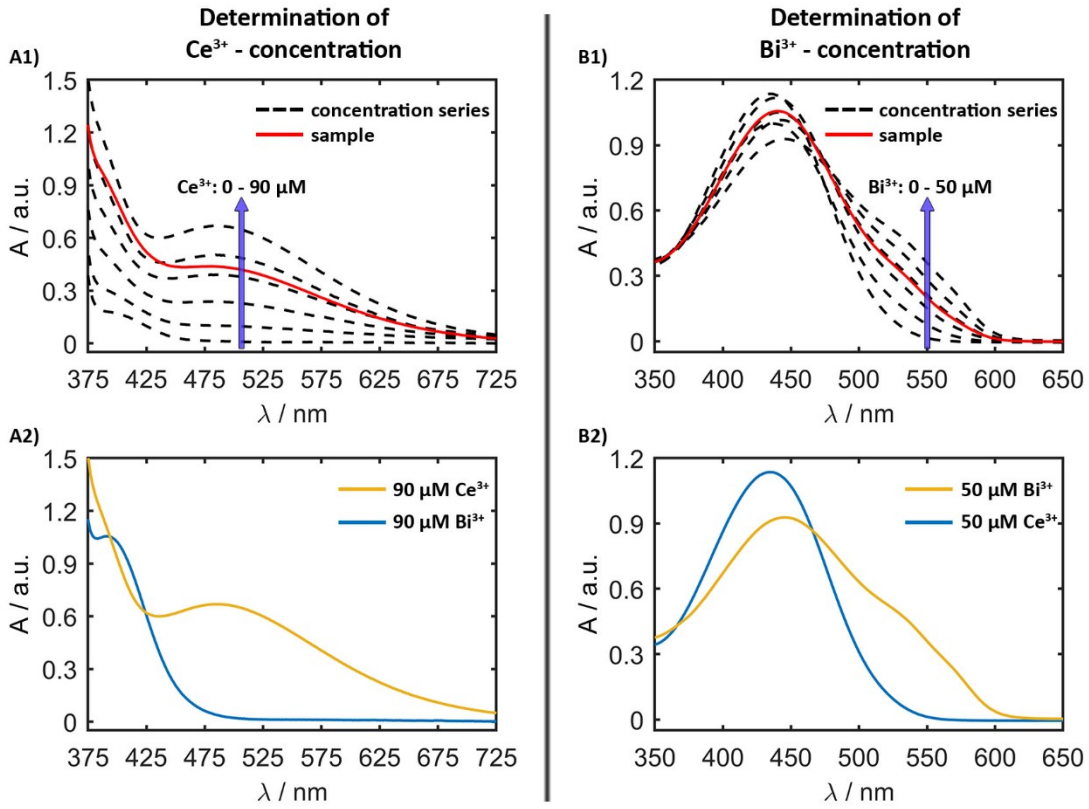

Figure S3. UV/Vis spectra of for Ce and Bi quantifications. (A1) Ce / 8-hydroxyquinoline spectra in chloroform as concentration series and sample measurements and (A2) spectrum of highest Ce concentration with equivalent bismuth blind spectrum. (B1) Bismuth / xylenolorange spectra in aqueous solution as concentration series and (B2) control spectra of highest Bi concentration with equivalent Ce blind spectrum.

Figure S4 shows both external calibrations and sample measurements with their respective linear regression. The cerium / 8-hydroxyquinoline solutions were measured at 505 nm and the bismuth / xylenolorange solutions at 550 nm. For the sample with the nominal composition of $Ce_{0.8}Bi_{0.2}O_{2-1.9}$ a ratio of Ce:Bi of 3.73 (Ce 0.7886±0.0113 / Bi 0.2114±0.0059) was determined by UV/Vis quantification. The metal content of the bulk samples compare well with the metal contents determined by EDX (Ce:Bi = 3.83).

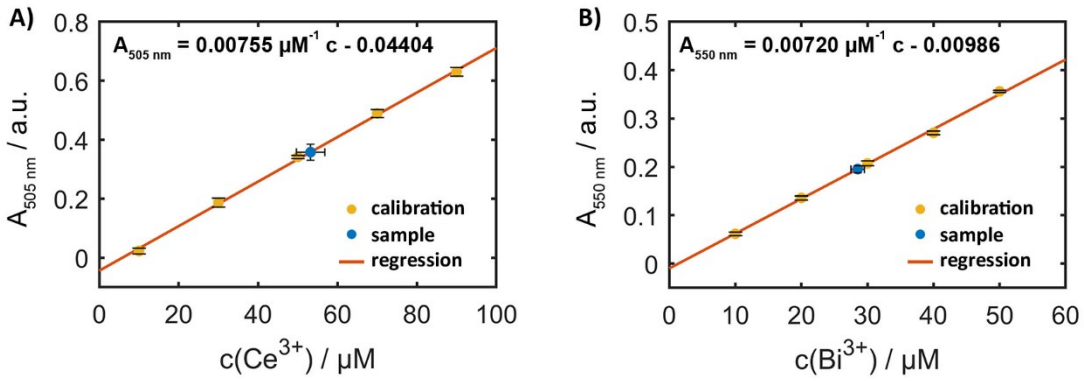

Figure S4. External calibrations for both metals together with the sample measurement ((A) cerium determination at 505 nm and (B) bismuth determination at 550 nm).

TEM microscopy

TEM images of the particles obtained from the hydrothermal synthesis (Figure S5) show the morphology change of the particles from rod-like (unsubstituted particles) to a cube-like appearance. The diffraction patterns obtained by TEM diffraction show a similar behavior for all particles. The diffraction patterns were analyzed by a radial profile data processing performed with Fiji.[5,6] For higher bismuth contents during the low temperature synthesis the excess of bismuth is not incorporated into the particles. This is in agreement with the results of the powder diffraction studies (Figure 1 of the main manuscript), where a second phase appears for bismuth contents $n(\mathrm{Bi}) > 0.3$. The second phase is isolated from the bismuth substituted ceria nanophase.

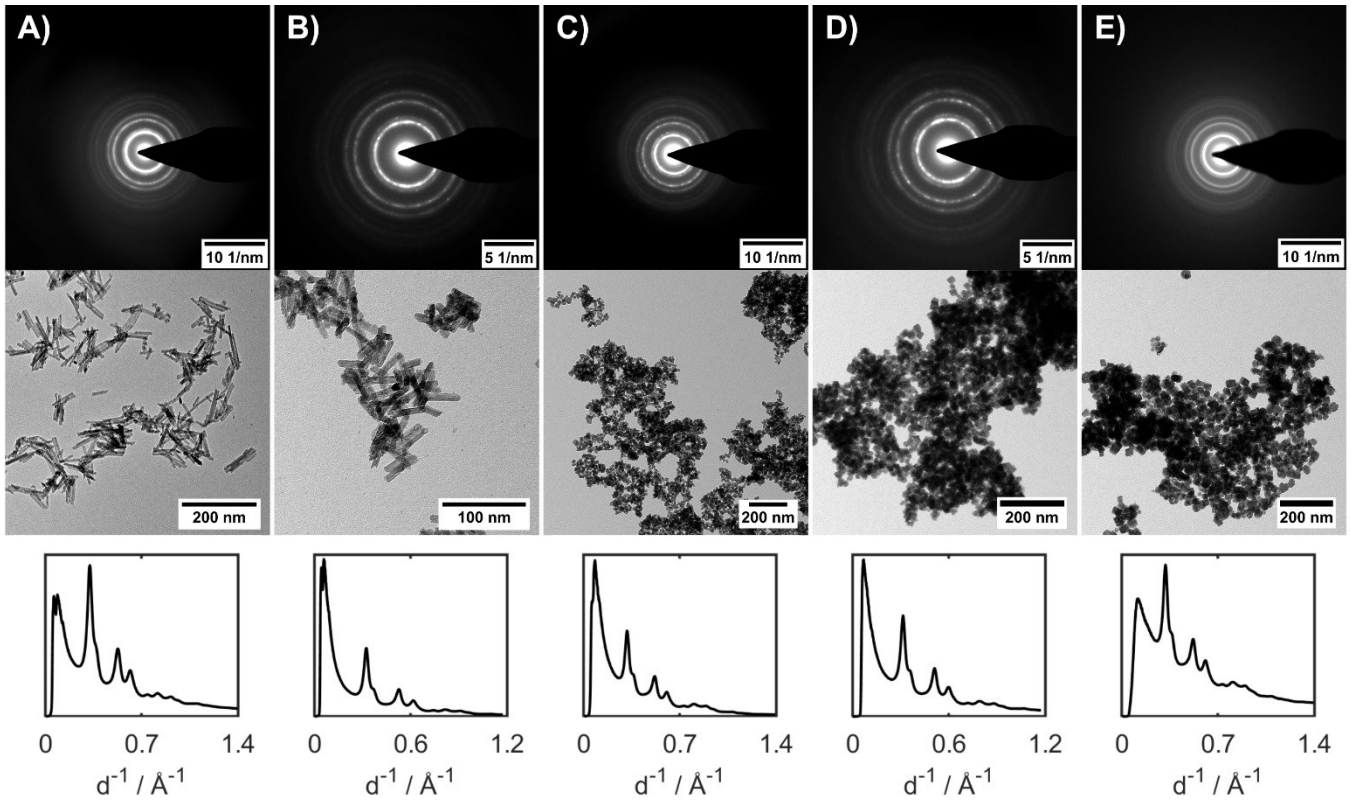

Figure S5. TEM images of substituted ceria nanoparticles and their respective TEM diffraction patterns analyzed with a radial profile function from A) $x = 0$ to E) $x = 0.4$ corresponding to the respective amount of bismuth ($Ce_{1-x}Bi_xO_{2-\delta}$).

SEM microscopy

A particle-dispersion in Ethanol was dropped onto silicon wafer (fixed onto a carbon pad) and dried overnight. SEM images were obtained using a FEI Nova NanoSEM 630 equipped with an EDAX-Pegasus X4M unit for the EDX measurements

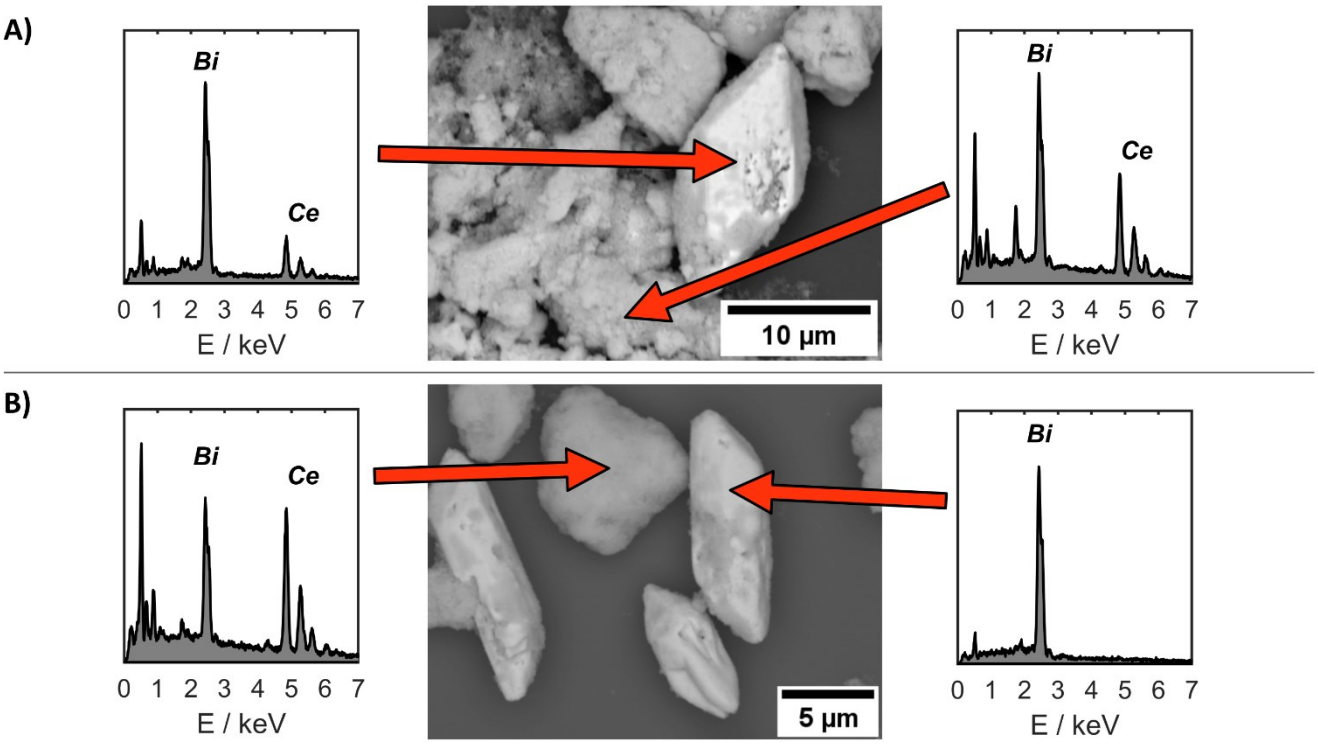

Figure S6. SEM microscopy of the ceria nanoparticle / bismite particle samples. (A) Synthesis with 0.3 eq Bi and (B) with 0.4 eq. Bi with respect to cerium.

XPS-measurements

For XPS measurements the samples $CeO_{2-\delta}$ and $Ce_{0.8}Bi_{0.2}O_{2-\delta}$ were pressed into indium foil and transferred into the XPS spectrometer (SPECS GmbH, Germany). In the survey scan of $CeO_{2-\delta}$ (Figure S7) only the XPS lines of Ce and O could be detected. The survey spectrum of $Ce_{0.8}Bi_{0.2}O_{1.90}$ (Figure S7) contained the XPS lines of Ce, Bi, and O. Both the measured electron binding energies and the spectral features of the Ce 3d spectrum (main-article Figure 3 B) agree with those of $CeO_{2-\delta}$.

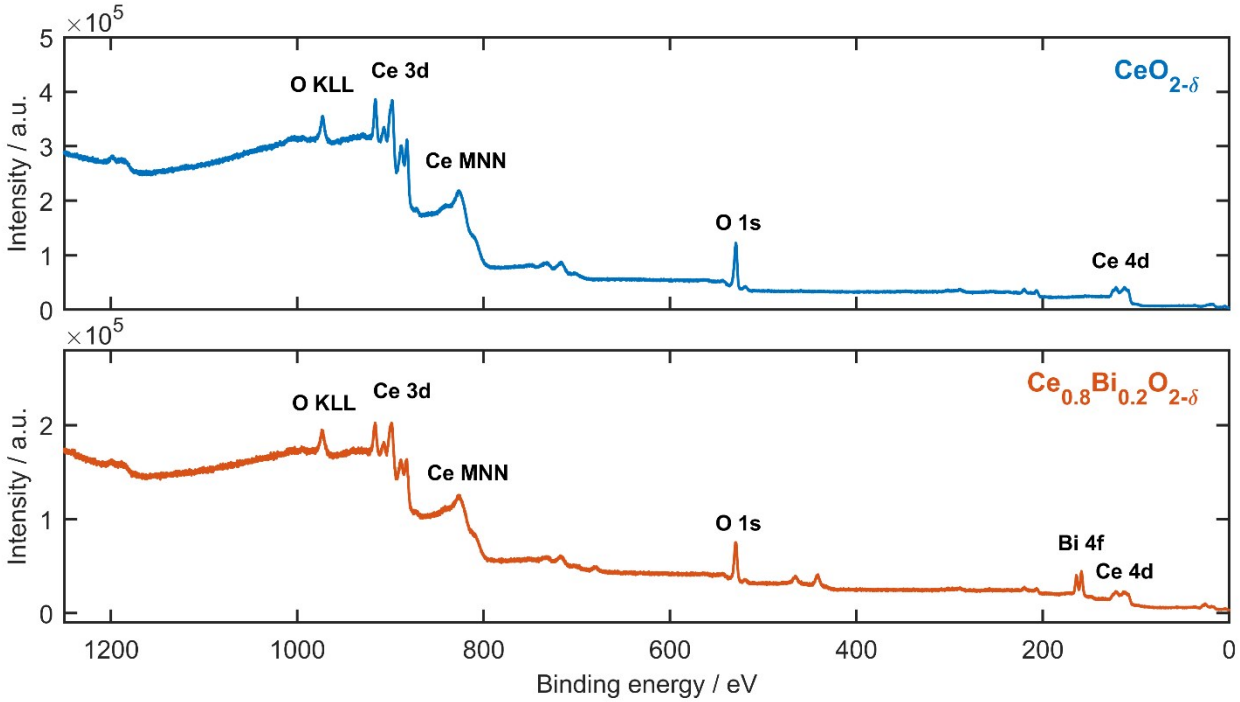

Figure S7. XPS survey spectrum of $CeO_{2-\delta}$ (top) and $Ce_{0.8}Bi_{0.2}O_{2-\delta}$ (bottom) using non-monochromatized Al Kα excitation.

Raman spectra

Raman spectra were recorded with an i-Raman BWS415-785S spectrometer equipped with a BAC100 fiber optical probe. The samples were placed onto a quartz plate and measured directly as powders. Data acquisition was done with the BWSpec (Spectral Acquisition Software) software from BWTEK.

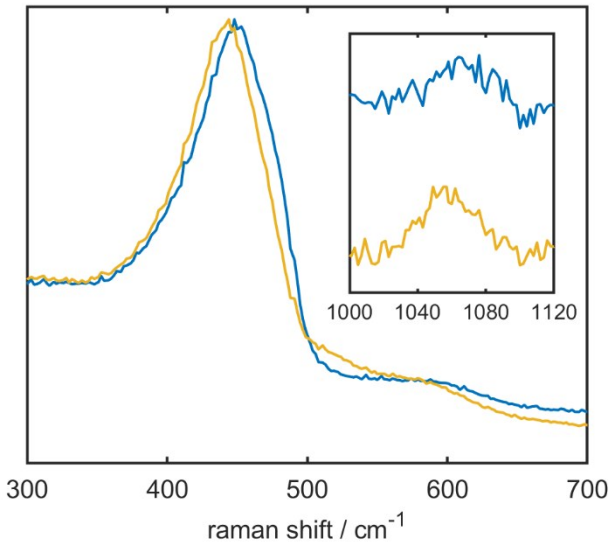

Figure S8. Raman-spectra of $CeO_{2-\delta}$ (blue) and $Ce_{0.8}Bi_{0.2}O_{2-\delta}$ (yellow) measured with a laser excitation of λ = 785 nm.

Monitoring the bromination of thymol by ^{1}H-NMR

Due to the low solubility of phenol red in aqueous media and the low solubility of potassium bromide in organic media thymol was used as substrate[9] to monitor the oxidative bromination. The reaction was carried out with a solution of 14.8 mg thymol, 12.4 mg KBr, 20 µL $HClO_4$ (35%), 20 µL H_2O_2 (35%) in a mixture of methanol (2 mL) and H_2O (200 µL). One reaction was carried out without catalyst addition and the other one with 3.4 mg of the bismuth substituted cerium oxide (Ce/Bi - 0.8/0.2). After 3 h both solutions were diluted to 10 mL with water and the thymol/bromothymol content was extracted with diethylether. After solvent evaporation the residue was dissolved in $CDCl_3$ and measured via ^{1}H-NMR.

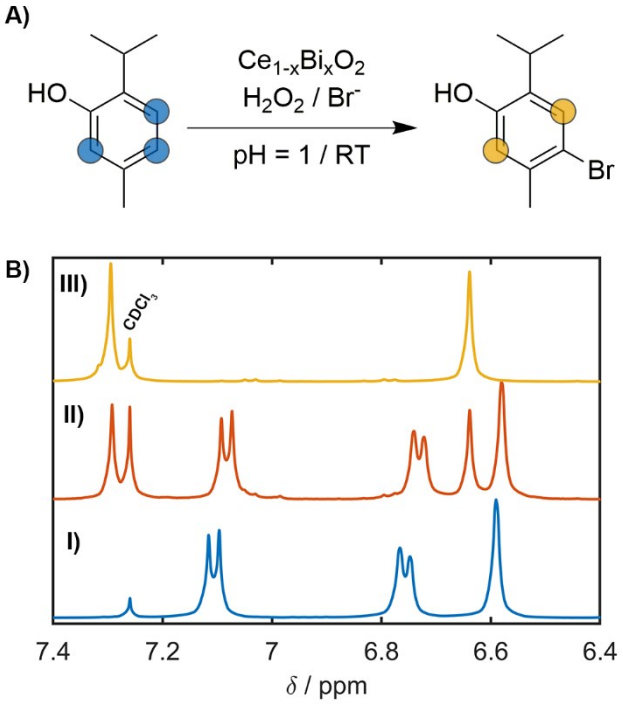

Figure 9. (A) Model bromination reaction with thymol as electron-rich substrate. (B) ^{1}H-NMR spectra of the aromatic region of the thymol substrate (I, reference), the product mixture in the absence of $Ce_{1-x}Bi_xO_2$ catalyst nanoparticles (II) and the reaction product in the presence of $Ce_{0.8}Bi_{0.2}O_{1.9}$ catalyst particles (III).

Phenol red activity screening tests (effect of daylight)

For the test of a blind activity by daylight a qualitative phenol red assay was performed. For all screening tests a mixture of the components was used as detailed in Table S4. The components were mixed, placed in 1.5 mL Eppendorf tubes and left undisturbed for 24 h. The evaluate the effect of light a second formulation was prepared that was protected from light with an aluminum foil.

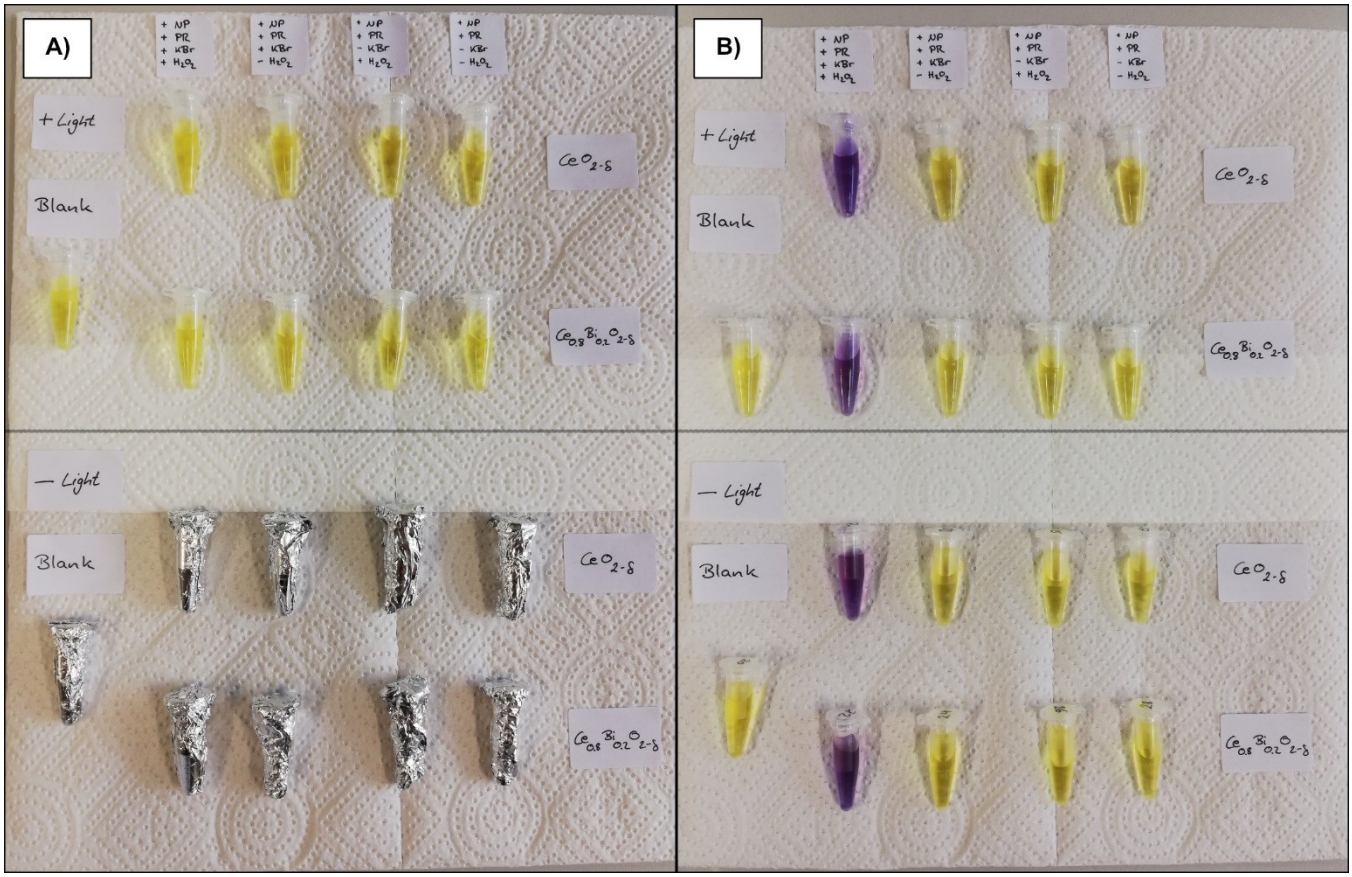

Figure S10. Phenol red assay under daylight conditions (top) and in the absence of light (wrapped in aluminum foil). (A) Immediately after addition of H_2O_2 and (B) after 24 h of reaction time.

BET surface measurements

The BET measurements were carried out with an Autosorb-6B surface area and pore size analyzer from Quantachrome. Sorption measurements were done with an appropriate amount (~100 mg) of sample. Prior to the measurements the samples were heated at 300 °C for 6 h under vacuum in the degassing step. The final weight of 94.4 mg for CeO_2 and for 101.7 mg $Ce_{0.8}Bi_{0.2}O_{1.9}$ were used for the BET surface determination. The samples were measured in triplicate with an eleven point multi-BET analyzer.

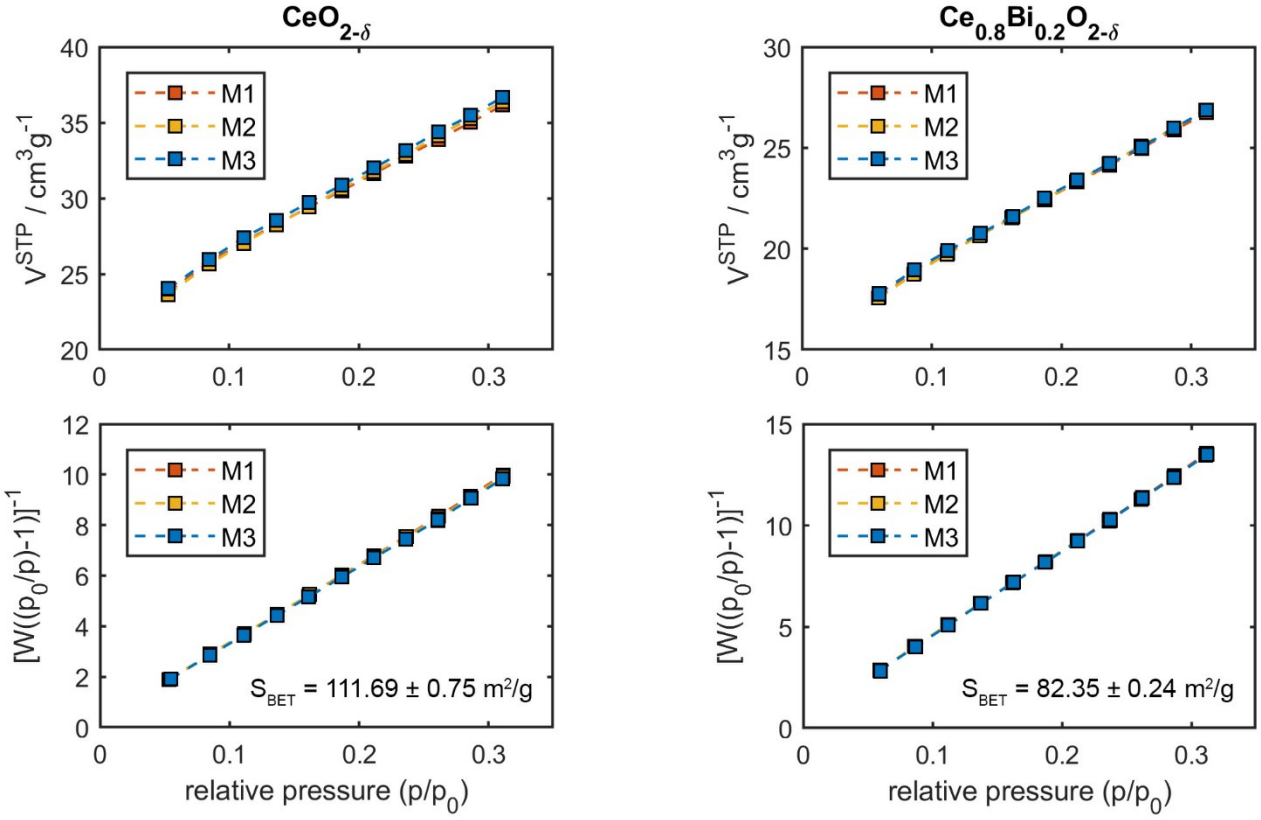

Figure S11. BET measurements of the particles and their respective plots. Left: $CeO_{2-\delta}$, right: $Ce_{0.8}Bi_{0.2}O_{2-\delta}$.

The surface area of the particles was determined with the ASiQwin software suite from Quantachrome using the BET Equation SI1.[7]

$$\frac{1}{W\left(\frac{p_0}{p}-1\right)} = \frac{C-1}{W_m C}\left(\frac{p}{p_0}\right) + \frac{1}{W_m C} \qquad \text{(SI 1)}$$

W describes the weight of adsorbed gas per gram of sample. W_m describes the weight of adsorbed gas per gram sample for a full monolayer coverage of the sample surface. The linear relationship of the formula is described for a p/p_0 range of 0.05–0.35. The resultant surface area is the sample specific surface area.

Powder diffraction and UV/Vis kinetics

Powder diffraction analysis with Rietveld refinements of the particles before and after catalysis were done by mixing about 10 mg of the particles with a solution of 15 mg phenol red, 1.4 g of KBr in 30 mL of MQ water. The catalysis was started by adding 30 µL of H_2O_2 (35%).

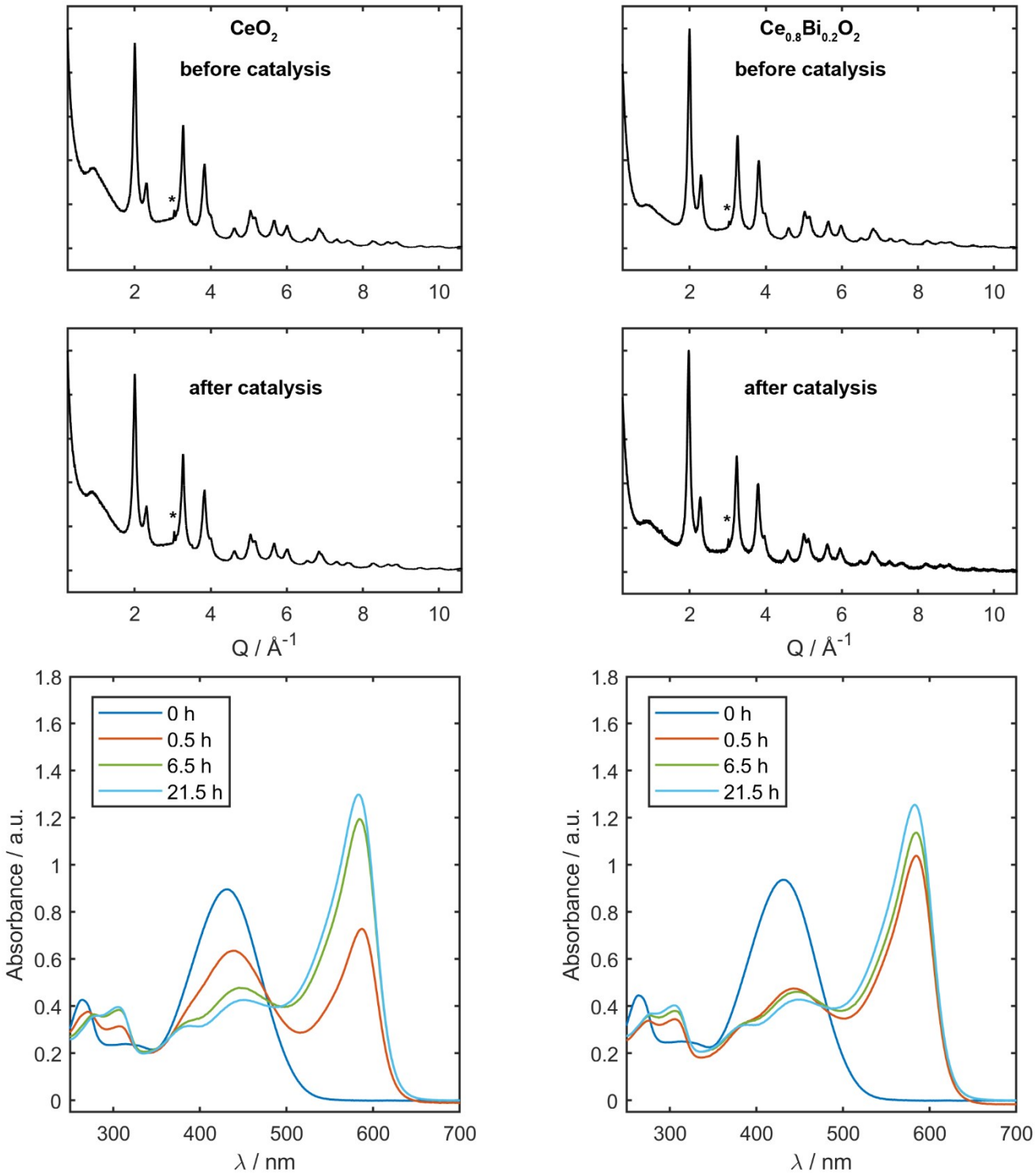

Figure S12. Rietveld measurements of the particles before and after the catalysis (catalysis progress is monitored by UV/Vis spectroscopy). Left: $CeO_{2-\delta}$ nanoparticles, right: $Ce_{0.8}Bi_{0.2}O_{2-\delta}$ nanoparticles. The "*" marked reflections are due to the sample preparation on acetate foil.

Fluoride as surface modifier

The effect of the surface potential on the catalytic activity was investigated by fluoride as surface modifier. The measurements were performed with concentrations of c(phenol red) = 50 µM, c(KBr) = 25 mM, β(NPs) = 25 µg mL^{-1} and c(H_2O_2) = 300 µM and variable amounts of sodium fluoride. The catalytic activity was evaluated at a wavelength of 590 nm prior to the formation of bromophenol blue in the range of 6 min by determination of the slope as the formation velocity (Figure 13 A1 and A2). Both materials show the effect of fluoride on the catalytic activity. Figure 13 B shows the ζ-potential for $Ce_{0.8}Bi_{0.2}O_{1.9}$. With increasing amounts of fluoride the potential shifts to more negative values. Figure 13 C shows the effect of fluoride modelled with an IC_{50} approach for activity inhibition (asymmetric n-factor due to non-ideal inhibition conditions).[8] The n-factor shows that the inhibition is non-ideal because $n \neq 1$. The data show a poisoning effect of the ζ-potential on the reactivity.

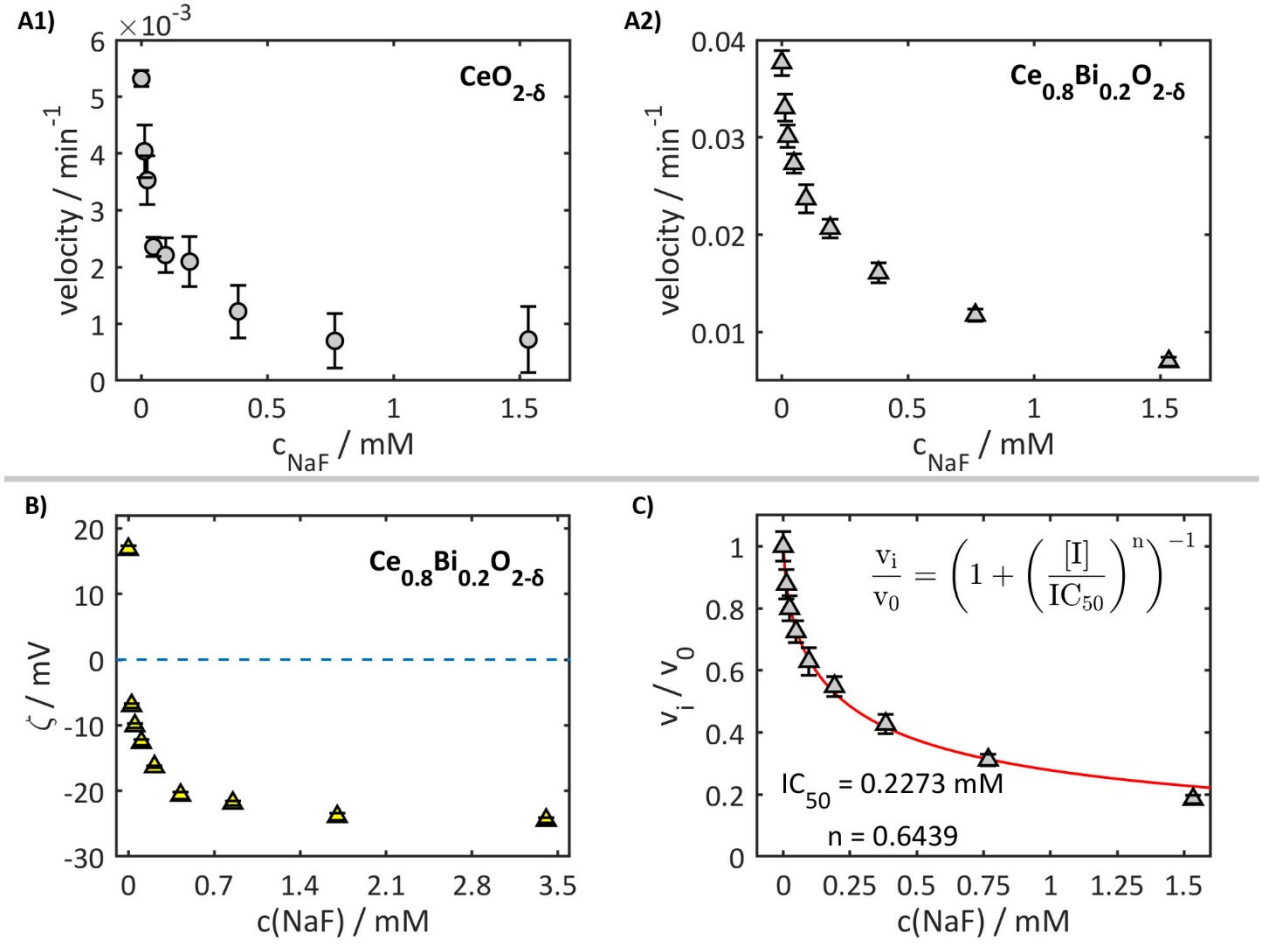

Figure S13. Effect of fluoride on the catalytic activity of $CeO_{2-\delta}$ (A1) and $Ce_{0.8}Bi_{0.2}O_{1.9}$ (A2) particle (c(phenol red) = 50 µM / c(KBr) = 25 mM / β(NPs) = 25 µg mL-1 / c(H_2O_2) = 300 µM). (B) Measurements of the ζ-potential for $Ce_{0.8}Bi_{0.2}O_{1.9}$. (C) IC_{50} approach to analyze the poisoning effect of fluoride on the catalytic activity of $Ce_{0.8}Bi_{0.2}O_{1.9}$.

Preparation and SEM Measurements of the polymer beads

The polymer beads were prepared by phase inversion from a solution of polyethersulfone (ω(PES) = 18.3wt%) and polyvinylpyrrolidone (ω(PVP) = 6.8wt%) in dimethylacetamide.[10–13] The solution was stirred overnight and left unperturbed for several hours for degassing. For the preparation of the composites, an appropriate amount of nanoparticles was added to the polymer solution. The mixture was stirred overnight, and the composite solution was allowed to settle for a few hours. The mixture was then dropped into a water / ethanol solution (ethanol: 27% v/v) through a syringe (27G).

SEM measurements were done with a FEI Nova NanoSEM630 equipped with an EDAX Pegasus X4M unit for EDX measurements. To show the incorporation of the particles, the polymers were frozen in liquid nitrogen. After 10 min of freezing time the beads were cut into half with a scalpel. The SEM and EDX measurements were done under water pressure (50 Pa) in order to prevent surface charging with a vCD (Low-kV, High-contrast Detector) detector.

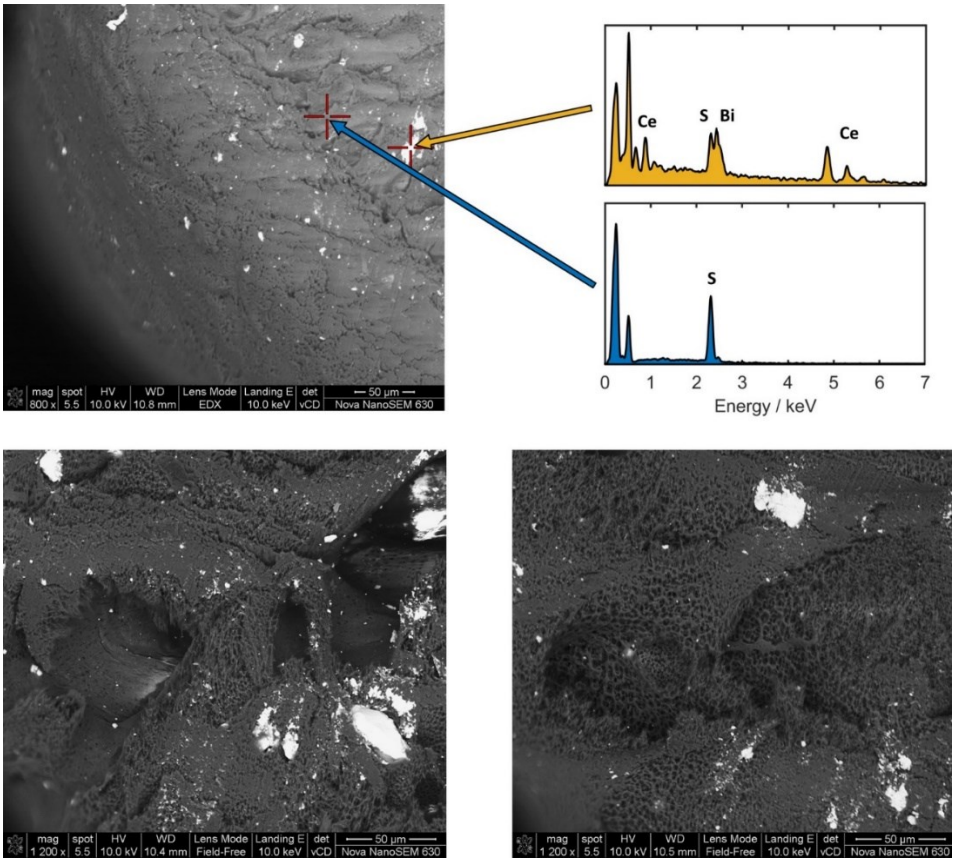

Figure S14. SEM / EDX measurements of the polymer beads with incorporated $Ce_{0.8}Bi_{0.2}O_{1.9}$ particles.

The EDX signal Figure 14 was processed using a Savitzky-Golay Filter (Matlab polynomial order 3 / frame length 11) for smoothing the data because of a low signal intensity due to the 50 Pa water pressure.[14]

The bright areas in Figure S14 show the presence of the heavy elements Ce and Bi. The beads have a porous structure, which allows for molecular diffusion.

Bromination of phenol red with polymer beads

For the flow cell measurements polymer beads with a mass content of 13 wt% nanoparticles (with respect to the amount of PES) were prepared. These beads were washed 10 times with water under ultrasonication (1 min) to produce the porous surface structure. The polymer beads were freeze dried and packed into a 1 mL syringe as column. For the reaction, a mixture of 32.5 mL of water and 6.6 mL of KBr (300 mM solution) was passed through the column for a baseline measurement. Afterwards, 3.3 mL of phenol red (1 mM solution) were added, and the mixture through the column and the column was equilibrated for 5 min. Subsequently, 2 mL of H_2O_2 (30 mM solution) were added to start the kinetic measurement.

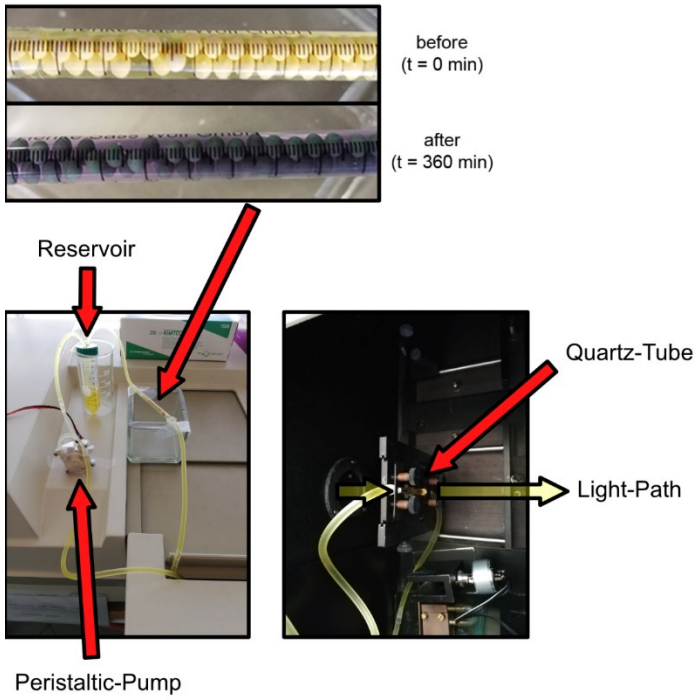

Figure S15. Activity measurements for $Ce_{0.8}Bi_{0.2}O_{1.90}$ loaded PES polymer beads in UV/Vis flow-cell.

Product characterization by NMR

A 3 mL syringe was packed with $Ce_{0.8}Bi_{0.2}O_{1.90}$ /PES beads (~15 wt% particles) and a catalysis volume of 100 mL was passed through the column (2.2 mg (6.2 µmol) phenol red / 336 mg (2.8 mmol) KBr in 100 mL MQ-water). The adsorption/desorption was performed by cycling the solution for 30 min. The catalysis was started by injection of 7.7 µL (~90 µmol) of H_2O_2 (35%). After 240 min of reaction time the solution was removed and collected. Adsorbed TBPB was collected by cycling 30 mL of MQ-water for 30 min through the cell. Both solutions were combined to extract TBPB. Figure S16 shows the UV/Vis profile.

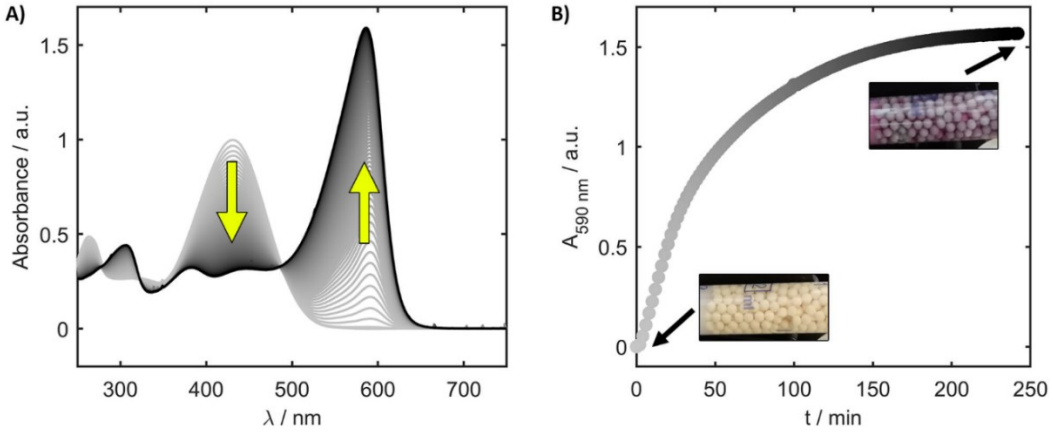

Figure S16. UV/Vis-spectra of the flow cell catalysis.

Subsequently, TBPB was extracted by washing the aqueous phase (4 times each) with 10 mL of a tetra-n-octylammoniumbromide/chloroform solution (0.25 g L^{-1}). The organic phase was dried with sodium sulphate, filtered and evaporated to dryness. The blue residue was dissolved in DMSO-d_6 and analyzed by NMR.

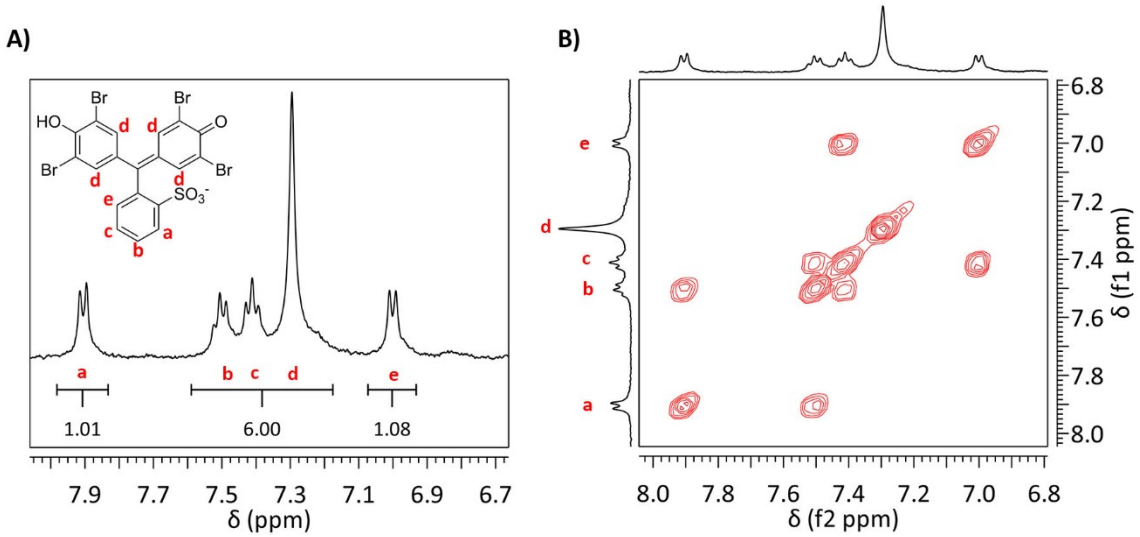

Figure S17. NMR-spectrum of the extracted product. (A) Spectrum of the aromatic region with integrals corresponding to the number of hydrogen atoms. (B) ^{1}H-^{1}H-COSY spectrum of the aromatic region.

PES blind activity

For the evaluation of a possible PES polymer blind activity the phenol red assay was run over 24 h of reaction time with and without incorporated particles. For the measurements, PES polymer beads in the absence and in the presence of 0.5 wt% of the particle species ($CeO_{2-\delta}$ and $Ce_{0.8}Bi_{0.2}O_{1.9}$ with respect to the amount of PES in the casting solution) were produced. The amount of particles was chosen to match the reaction time of 24 h. The polymer beads were incubated for 24 h in a solution of 1 mL of H_2O, 100 µL of KBr (300 mM stock solution) and 62.5 µL of phenol red (1 mM stock solution). After 24 h the supernatant was analyzed by UV/Vis spectroscopy. Parallel trials were set up in the presence and in the absence of H_2O_2 (30 mM stock solution). The reaction mixture without PES beads showed no reaction in the presence and in the absence of hydrogen peroxide (Figure S18). No reaction was observed with blank PES polymer in the absence of ceria particles. The polymer composites with incorporated ceria particles showed a positive reaction only in the presence of H_2O_2. The $Ce_{0.8}Bi_{0.2}O_{1.9}$ particles showed an enhanced activity compared to the $CeO_{2-\delta}$ particles.

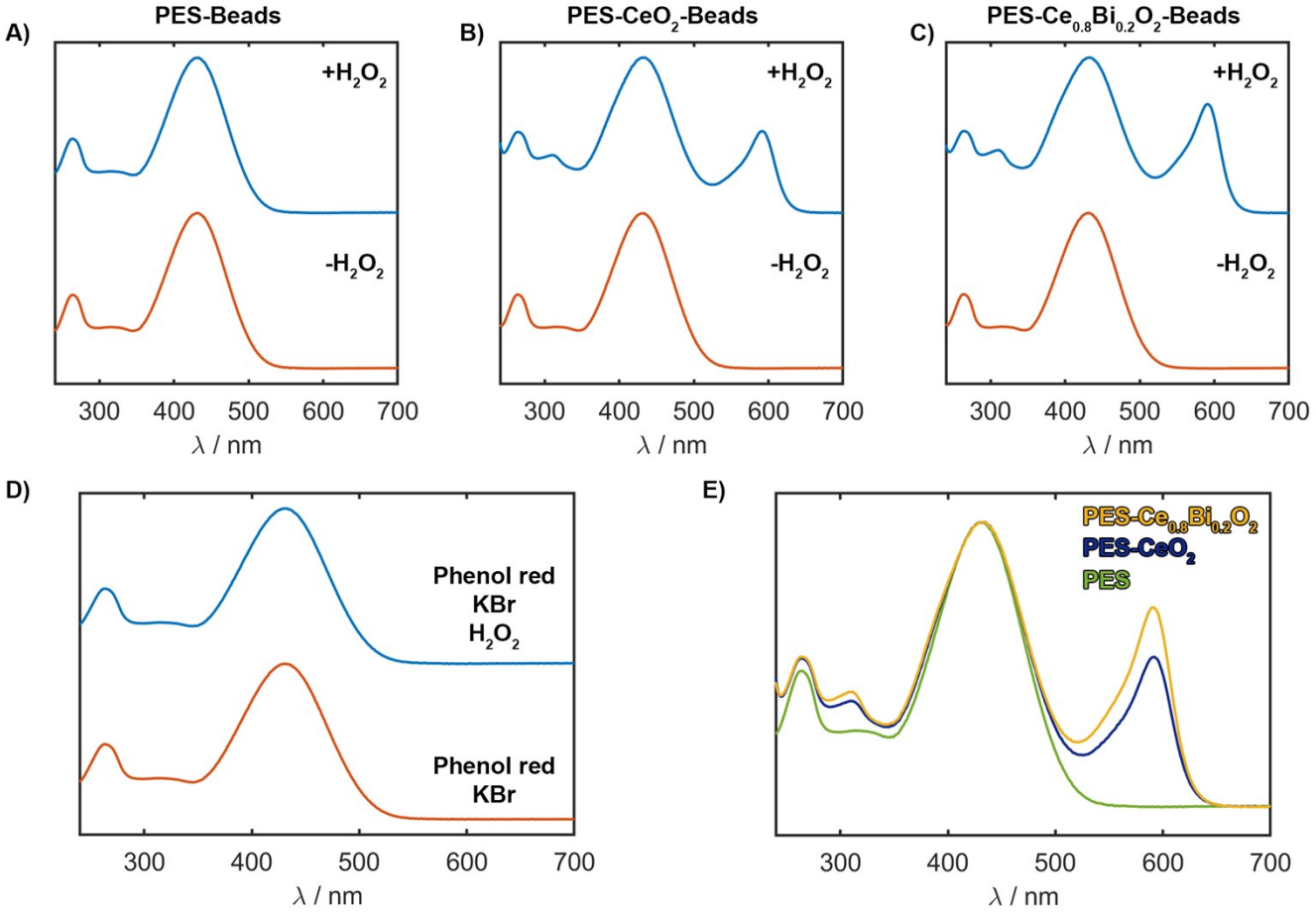

Figure S18. Blind activity measurements of the PES beads with and without nanoceria. (A) PES beads blind activity. (B) PES beads with incorporated $CeO_{2-\delta}$ particles. (C) PES beads with incorporated $Ce_{0.8}Bi_{0.2}O_{1.90}$ particles. (D) Reaction solution of the phenol red assay with and without the addition of peroxide. (E) UV-vis spectra of the supernatant of PES beads with incorporated $CeO_{2-\delta}$ and $Ce_{0.8}Bi_{0.2}O_{1.90}$ particles 24 h after adding H_2O_2.

Preparation of the polymer composite membranes

The preparation of the polymer membranes for the biofilm formation test were prepared in analogues form as stated in the part -Preparation and SEM Measurements of the polymer beads-. The membranes were produced via phase inversion using a solution of polyethersulfone (ω(PES) = 18.3wt%) and polyvinylpyrrolidone (ω(PVP) = 6.8wt%) in dimethylacetamide.[10–13] The polymer solution was stirred overnight and left undisturbed for several hours (degassing). For the polymer-nanoparticle composite membranes an appropriate amount of nanoparticles was then added to the polymer solution (10 wt% particles $CeO_{2-\delta}$ and $Ce_{0.8}Bi_{0.2}O_{1.90}$ with respect to the amount of PES) and the mixture was stirred again overnight and left undisturbed afterwards for a few hours. For the membrane production an aliquot of the mixture was spread onto a glass plate via a doctor blade (266 µm). After 30 seconds at air the polymer mixture was coagulated for several minutes in a water / ethanol bath (ethanol: 27% v/v). The resulting thin polymer sheet was washed several times first with a water / ethanol solution and afterwards with MilliQ water. The membranes were then left overnight in MilliQ water prior to being used for the biotest.

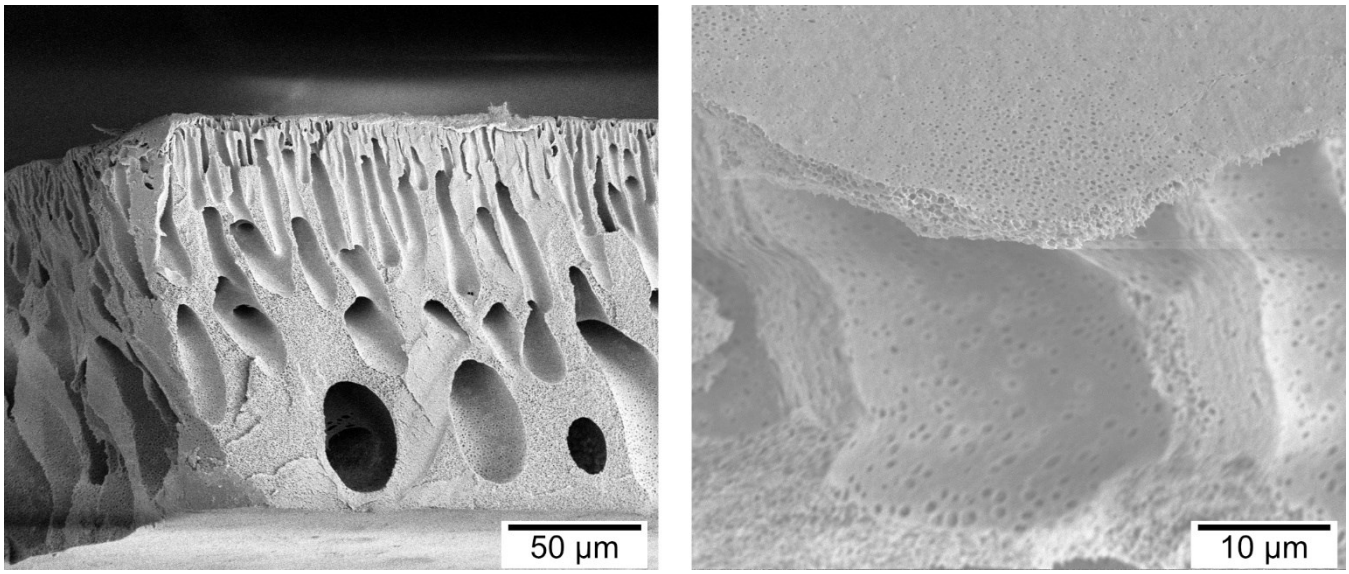

Figure S19. Side and top view of PES membranes with incorporated $Ce_{0.8}Bi_{0.2}O_{1.90}$ nanoparticles.

Rietveld measurements

Table S1. Parameters of the Rietveld refinements.

	$CeO_{2-\delta}$	$Ce_{0.8}Bi_{0.2}O_{2-\delta}$
Device	STOE Stadi P, transmission geometry	
Wavelength / Å	0.7093 ($MoK\alpha_1$)	
Scan range, mode	$1.5 \leq 2\Theta/° \leq 73.5$, $\Delta 2\Theta/° = 0.015$, continous scan	
Refinement	Full pattern, Rietveld	
Programm	TOPAS Academic V6	
Parameters / background	18 / 13	
Profile	WPPM, cubes, log normal distribution	
Space group	$Fm\bar{3}m$ (SG 225)	
Lattice parameter / Å	a = 5.4325(2)	a = 5.4552(1)
average crystallite size / nm	5.2(1)	5.8(1)
B_{eq} /Å^2	0.91(2)	2.52(3)

XPS spectroscopy

Surface charging was corrected by setting the binding energy of the Ce $3d_{5/2}$ peak of $CeO_{2-\delta}$ to 882.3 eV.[15,16] Measured electron binding energies E_b are compiled in Table S2. Peak areas and positions of the spectral components were treated as adjustable parameters. During the fit of the Ce 3d and Bi 4f spectrum the FWHM of the corresponding pairs of peaks was coupled to the corresponding values.

Table S2. Electron binding energies E_b (eV) for the unsubstituted ($CeO_{2-\delta}$) and substituted ($Ce_{0.8}Bi_{0.2}O_{1.90}$) samples and comparison with literature values. The FWHM values are given in parentheses.

Sample	**Ce $3d_{5/2}$**	**Sat1**	**Sat2**	**Bi $4f_{7/2}$**	**O 1s (CeO_2)**	**O 1s (OH^-)**	**O 1s (H_2O)**
CeO_2*	882.3 (2.7)	888.1 (5.7)	897.9 (2.6)		529.3 (1.8)	531.0 (1.8)	533.2 (1.8)
$Ce_{0.8}Bi_{0.2}O_{1.90}$*	882.3 (3.2)	888.2 (5.8)	898.0 (3.2)	158.4 (2.1)	529.2 (2.4)	531.2 (2.4)	-
CeO_2[15]	882.3	888.8	898.0		529.5		
CeO_2[16]	882.3 (1.5)	889.1	898.3		529.4 (1.0)	531.7 (2.0)	
Bi_2O_3[17]				158.5	529.1		

*E_b of Ce $3d_{5/2}$ in CeO_2 was set to 882.3 eV[15,16] to correct for electrostatic sample charging. The error in E_b is ±0.1 eV.

XPS spectroscopy

The binding energies E_b of O 1s and Ce $3d_{5/2}$ are compiled in Table S2 and compared to literature values for $CeO_{2-\delta}$. Both, electron binding energies and the spectral features of the Ce 3d spectrum (main manuscript, Figure 3 A) confirm the presence of Ce^{4+} at the particle surface. A contribution of Ce^{3+} could not be detected by XPS. The O 1s spectrum of $CeO_{2-\delta}$ (main manuscript, Figure 3 C) showed three components: Besides oxide oxygen (~70%), hydroxyl groups (~26%) and water (~4%) are present at the $CeO_{2-\delta}$ surface (Table S3). Ce^{3+} could not be detected at the sample surface by XPS. The O 1s spectrum of $Ce_{0.8}Bi_{0.2}O_{2-\delta}$ was fitted with two components corresponding to ~87% of oxide and ~13% of hydroxyl groups (Table S3). From the relative O 1s and Ce $3d_{5/2}$ peak intensities measured for $CeO_{2-\delta}$ (assuming an ideal O:Ce ratio of 2.0 at the surface) a XPS sensitivity factor SF = 0.2444 was derived. Using this SF and the measured O 1s and Ce $3d_{5/2}$ peak areas, the atomic O:Ce ratio at the $Ce_{0.8}Bi_{0.2}O_{1.90}$ surface was 2.7. Within experimental uncertainty, this value agrees with the expected value of 2.5 for a composition $Ce_{0.8}Bi_{0.2}O_{1.90}$. E_b of the Bi $4f_{7/2}$ electrons in $Ce_{0.8}Bi_{0.2}O_{1.90}$ was 158.4 eV. This agrees with the values reported for Bi_2O_3[17] (Table S2).

Table S3. Relative intensities (%) of the O 1s components for both samples.

Sample	O 1s (CeO_2)	O 1s (OH^-)	O 1s (H_2O)
$CeO_{2-\delta}$	70	26	4
$Ce_{0.8}Bi_{0.2}O_{1.90}$	87	13	0

The relative error is ±5%.

Phenol red activity screening tests (effect of daylight)

Table S4. Concentrations of components for phenol red assays**.**

Component	Blank	Column			
		1st	2nd	3rd	4th
MQ-Water	1 mL	1 mL	1 mL	1 mL	1 mL
phenol red (1 mM)	100 µL	100 µL	100 µL	100 µL	100 µL
KBr (300 mM)	200 µL	200 µL	200 µL	-	-
ceria nanoparticle (1 mg mL^{-1})	-	62.5 µL	62.5 µL	62.5 µL	62.5 µL
H_2O_2 (30 mM)	25 µL	25 µL	-	25 µL	-

References

(1) A. A. Coelho, *J. Appl. Crystallogr.* 2018, **51** (1), 210–218.

(2) R. W. Cheary, A. A. Coelho, *J. Appl. Crystallogr.* 1992, **25** (2), 109–121.

(3) O. G. Koch, G. A. Koch-Dedic, *Handbuch Der Spurenanalyse: Die Anreicherung Und Bestimmung von Spurenelementen Unter Anwendung Chemischer, Physikalischer Und Mikrobiologischer Verfahren*; Springer Berlin Heidelberg, 1974.

(4) E. B. Sandell, C*olorimetric Determination of Traces of Metals*; Chemical analysis: A series of monographs on analytical chemistry and its applications; Interscience Publishers, 1950.

(5) C. T. Rueden, J. Schindelin, M. C. Hiner, B. E. DeZonia, A. E. Walter, E. T. Arena, K. W. Eliceiri. *BMC Bioinformatics* 2017, **18** (1), 529.

(6) J. Schindelin, I. Arganda-Carreras, E. Frise, V. Kaynig, M. Longair, T. Pietzsch, S. Preibisch, C. Rueden, S. Saalfeld, B. Schmid, J.-Y. Tinevez, D. J. White, V. Hartenstein, K. Eliceiri, P. Tomancak, A. Cardona, *Nat. Methods* 2012, 9 (7), 676–682.

(7) G. Fagerlund, *Matériaux Constr.* 1973, 6 (3), 239–245.

(8) R. A. Copeland, *Enzymes: A Practical Introduction to Structure, Mechanism, and Data Analysis*; Wiley, 2004.

(9) F. Sabuzi, E. Churakova, P. Galloni, R. Wever, F. Hollmann, B. Floris, V. Conte, *Eur. J. Inorg. Chem.* 2015, 2015 (21), 3519–3525.

(10) A. Sotto, G. Orcajo, J. M. Arsuaga, G. Calleja, J. Landaburu-Aguirre, *J. Appl. Polym. Sci.* 2015, **132** (21), https://doi.org/10.1002/app.41633.

(11) J.-F. Li, Z.-L. Xu, H. Yang, C.-P. Feng, J.-H. Shi, *J. Appl. Polym. Sci.* 2008, **107** (6), 4100–4108.

(12) B. Vatsha, J. C. Ngila, R. M. Moutloali, *Phys. Chem. Earth, Parts A/B/C* 2014, **67–69**, 125–131.

(13) M. Peydayesh, M. Bagheri, T. Mohammadi, O. Bakhtiari, *RSC Adv.* 2017, **7** (40), 24995–25008.

(14) A. Savitzky, M. J. E. Golay, *Anal. Chem.* 1964, **36** (8), 1627–1639.

(15) Y. A. Teterin, A. Y. Teterin, A. M. Lebedev, I. O. Utkin, *J. Electron Spectros. Relat. Phenomena* 1998, **88–91**, 275–279.

(16) K. I. Maslakov, Y. A. Teterin, A. J. Popel, A. Y.Teterin, K. E. Ivanov, S. N. Kalmykov,V. G. Petrov, P. K. Petrov, I. Farnan, *Appl. Surf. Sci.* 2018, **448**, 154–162.

(17) T. P. Debies, J. W. Rabalais, *Chem. Phys.* 1977, **20** (2), 277–283.